

# Quantum simulation with ions in micro-fabricated Penning traps

S. Jain, J. Alonso, M. Grau and J. P. Home

*Institute for Quantum Electronics, ETH Zürich, Otto-Stern-Weg 1, 8093 Zürich, Switzerland*

We propose the use of 2-dimensional Penning trap arrays as a scalable platform for quantum simulation and quantum computing with trapped ions. Using realistic experimental parameters, we show that large arrays of micro-structured electrodes defining static quadrupoles can be embedded in a magnetic field to form closely-spaced trap sites with axial, magnetron and cyclotron motions exhibiting dipolar coupling with rates significantly higher than expected decoherence channels. We give a general approach to solving the normal modes of many ions in Penning trap arrays, which we use to compare the modes under various geometrical constraints. This approach allows us to derive a generalized multi-ion invariance theorem for stable motion even in the presence of trap imperfections. We show that laser fields allow tunable-range ferromagnetic and antiferromagnetic spin-spin couplings to be engineered, depending on which set of modes is used. The proposed setup allows higher ion density while avoiding a number of challenges which are present for radio-frequency traps, such as power dissipation and sensitivity to stray electric fields. It therefore becomes possible to envision an ion trap chip of  $1\text{ cm}^2$  which holds a system of 250,000 ions. The architecture and methods provided here could also greatly facilitate scaling in trapped-ion quantum computing.

The study of many-body physics in quantum mechanics is hindered by the inability of classical computing devices to store and manipulate the information required to specify these systems beyond about 50 spins [1, 2]. The possibility to overcome this limitation by using well-controlled quantum systems that can closely replicate the physics of interest under tunable conditions provides a new paradigm for many-body physics, which has stimulated a wide variety of both theoretical and experimental work [1, 3–5]. Many leading experimental results have been achieved using trapped-ions, which can be controlled with extremely high precision, and which have recently demonstrated controlled spin interactions and phase transitions in systems ranging from small ion strings to hundreds of ions [6, 7]. However these semi-rigid ion crystals, formed through the competing energy requirements of the global trapping potential and the Coulomb repulsion, intrinsically link the structure of the lattice to the oscillation frequencies of the normal modes of oscillation. This places restrictions on the models and frequencies which can be engineered. The geometry of the lattice is defined by the lowest-energy configuration, and thus for realizing both extended 2- and 1-dimensional crystals the anisotropy of the potential requires a large ratio between the curvature of the potentials in the reduced and extended dimensions. This has the result that a low-lying set of modes must exist aligned with the axis or axes along which the structure of the ion crystal has its greatest extent. For radio-frequency (r.f.) traps, optimal trapping for quantum control is achievable at the null of the radio-frequency electric field, which due to the constraints of Laplace’s equation can only be satisfied at specific isolated points in space or along a line. Stable trapping of two-dimensional crystals in Penning traps currently involves continuous rotation of the crystal in the plane perpendicular to the magnetic field, which creates additional challenges for high fidelity control.

An alternative to using bulk crystals is to utilize micro-fabricated ion traps with electrode structures on

the length scale of the inter-ion separation. For radio-frequency traps, this has been proposed to allow each ion in an array to be placed at a zero-dimensional r.f. field null, with the long-range Coulomb coupling providing links between the sites [8, 9]. This approach is experimentally challenging. One of the primary challenges is to achieve small site spacing such that the ions’ vibrations are strongly coupled, within the limitations of finite breakdown voltage for the radio-frequency trapping fields and the need to keep the ions far from the electrode surface in order to mitigate noise and allow free optical access for control fields [10–12]. A second is that the operation of such traps relies on the superposition of a static and radio-frequency quadrupole potential. Both of these are inhomogeneous and must be precisely aligned to avoid driven radio-frequency micromotion, which is challenging to achieve in the presence of stray charges on the electrode surfaces [13]. One approach to realize higher coupling rates at a given inter-site distance would be to use light particles, such as electrons [14, 15], but in practice the lack of laser cooling and manipulations restricts the available control relative to what is likely required for quantum computing and simulation [16, 17].

In this Letter, we propose to use micro-fabricated electrode structures to realize an array of *static* quadrupole centers, which are supplemented by a uniform magnetic field in order to realize a 2-dimensional (2-d) array of Penning traps for atomic ions. We investigate optimal electrode geometries, and demonstrate that for similar voltages and trap conditions, the Penning trap offers significantly higher ion densities and thus higher coupling. We give a general treatment of the motion of ions in Penning trap arrays, which allows us to investigate the nature of normal modes. We find that the motion of  $N$  coupled ions maps onto a quadratic eigenvalue problem, allowing a solution for both classical and quantum treatments, and provide a generalization of the single-ion invariance theorem for stable modes of motion [18, 19] to an arbitrary number of ions. We use this analysis to investigate the

normal modes of 2-d ion array systems. As an example of laser cooling in such an array, we numerically simulate Doppler cooling of a hexagonal unit cell, showing that all modes can be cooled with the addition of an axialization potential [20]. The strongly-coupled motional modes are well suited for quantum simulation of coupled oscillator systems, but with the addition of laser coupling to the internal states, also of Hamiltonians including spin-boson and spin-spin interactions [21]. As a test case for quantum simulations utilizing the internal states of the ions, we consider the possibility of realizing effective spin-spin interactions with tunable range between ions in the array.

## I. PENNING MICROTRAP ARRAY

The configuration that we propose is shown in figure 1. A periodic array of conducting electrodes is laid out on a planar trap structure, which is then placed in a large homogeneous magnetic field. The desirable electrode geometries will be considered in section III, but will have the same symmetry and periodicity as the desired ion lattice. Potentials are applied to the trap electrodes such as to form an array of static electric quadrupoles at a distance  $h$  above the trap surface. These, combined with the homogeneous magnetic field, provide three-dimensional confinement of a single ion at each site. The basis for interesting physics in such a setting is the long-range Coulomb interaction, which couples the oscillations of individual ions at different sites.

## II. DIPOLAR ION-ION COUPLING.

The Coulomb interaction defines both the equilibrium positions and the collective oscillations of the ions around these positions. For an infinite lattice, the equilibrium positions will align with the centers of the quadrupole potentials. For a finite lattice, this will not be the case, but additional potentials should allow compensation of the discrepancy. For quantum simulations, the central component is the coupled oscillations of the ions. While for an ion oscillating along a single spatial axis it is simple to think of the oscillating charge distribution as an oscillating dipole potential and thus that the ions are coupled through something similar to a dipole-dipole coupling, the types of motion exhibited by ions in a Penning trap are less straightforward.

To get a feeling for the nature of this coupling, we first consider for the moment a simplified setting, in which each ion is trapped in a symmetric static quadrupole potential  $m\omega_z^2/2(z^2 - (x^2 + y^2)/2)$  for ions of mass  $m$  and charge  $e$  embedded in a magnetic field of strength  $B_0$  aligned along the  $z$  axis. At a single site, the potential

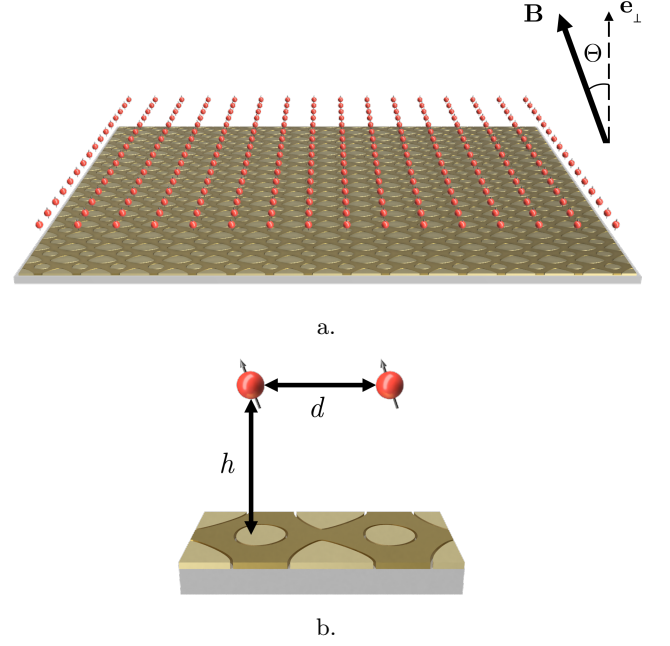


FIG. 1. Proposed array of Penning microtraps. The magnetic field  $\mathbf{B}$  makes an angle  $\Theta$  with  $\mathbf{e}_\perp$ , the vector normal to the lattice plane in which all of the ions lie. The ion separation is given by the electrode pattern. The critical parameter for the ion-ion interaction is the separation of neighboring sites  $d$ , while the distance from the surface  $h$  strongly affects the level of noise from fluctuating electric fields [22]

and magnetic field give rise to a Hamiltonian

$$\hat{H}_s = \hbar\omega_1 (\hat{a}_x^\dagger \hat{a}_x + \hat{a}_y^\dagger \hat{a}_y + 1) + \hbar\omega_z (\hat{a}_z^\dagger \hat{a}_z + 1/2) + \frac{\hbar\omega_c}{2} (\hat{a}_x^\dagger \hat{a}_y + \hat{a}_y^\dagger \hat{a}_x), \quad (1)$$

where  $\omega_1 = \sqrt{\omega_c^2 - 2\omega_z^2}$  and  $\omega_c = eB_0/m$  is the bare cyclotron frequency. Under the appropriate transformation [19], this Hamiltonian can be re-written as a sum of three independent harmonic oscillators

$$\hat{H}_s = \sum_\nu \hbar\omega_\nu (\hat{a}_\nu^\dagger \hat{a}_\nu + 1/2), \quad (2)$$

where  $\nu \in \{z, +, -\}$  and  $\omega_\pm = (\omega_c \pm \omega_1)/2$  are the frequencies of the modified cyclotron motion and magnetron motion respectively. Let us now consider two such sites labelled by indexes  $i$  and  $j$  containing ions with equilibrium positions separated by the vector  $\mathbf{R}_{ij,0} = R_{ij,0}(\sin(\theta_{ij}) \cos(\phi_{ij}), \sin(\theta_{ij}) \sin(\phi_{ij}), \cos(\theta_{ij}))$  which has magnitude  $R_{ij,0}$  and makes an angle  $\theta_{ij}$  with the magnetic field. For the current argument, let us work in the approximation that the motion of the ions can be assumed to be a small perturbation which is well described using a second order expansion of the Coulomb interaction about the equilibrium positions. Moving to a rotating frame with respect to  $\hat{H}_s$  for the operators at each of the sites and further assuming that the difference frequency between the bare modes is much larger

than the respective exchange frequencies for the different modes, we find the Coulomb interaction Hamiltonian

$$\hat{H}_{c,ij} = \sum_{\nu} \hbar \Omega_{\nu,ex}^{ij} K_{\nu} \left( \hat{a}_{\nu,i}^{\dagger} \hat{a}_{\nu,j} + \hat{a}_{\nu,j}^{\dagger} \hat{a}_{\nu,i} \right) - \sum_{\nu} \hbar \Omega_{\nu,ex}^{ij} K_{\nu} \left( \hat{a}_{\nu,i}^{\dagger} \hat{a}_{\nu,i} + \hat{a}_{\nu,i} \hat{a}_{\nu,i}^{\dagger} \right) \quad (3)$$

where  $K_z = -K_{\pm} = 1 - 3 \cos^2(\theta_{ij})$ . The first term corresponds to hopping of excitations between the sites, while the second gives the modification of the on-site energy due to the static potential of the other ion. The respective coupling strengths for hopping of vibrational oscillations from one ion to another are given by the exchange frequencies

$$\Omega_{\nu,ex}^{ij} = \frac{e^2}{4\pi\epsilon_0 m \omega'_{\nu} R_{ij,0}^3} \quad (4)$$

where  $\omega'_z = \omega_z$  and  $\omega'_+, \omega'_- = \omega_1$ .

The coupling Hamiltonian has a dipolar form for all modes. The sign of the coupling for the magnetron and cyclotron motions is inverted with respect to the axial motion. For each type of motion the orientation of the effective dipole is along the magnetic field axis. While this is expected for the axial oscillation, for the other modes this is less intuitive, since it corresponds to a direction perpendicular to the plane of oscillation of both the cyclotron and magnetron motions. When the coupling above is generalized to a two-dimensional lattice of sites, the anisotropy of the interactions in the lattice plane depends on the angle  $\Theta$  between the magnetic field and the lattice normal. For  $\Theta = 0^\circ$  the interactions are isotropic because  $\theta_{ij} = \pi/2$  for all directions within the plane. For  $\Theta = 90^\circ$   $\theta_{ij}$  varies between 0 and  $2\pi$ , thus the interactions are anisotropic.

### III. OPTIMAL ELECTRODE GEOMETRIES

From equation 4 above, it is clear that the  $1/R_{ij,0}^3$  nature of effective couplings between the ions favors forming closely-spaced ion arrays. Although this can be achieved by scaling the size of the whole trapping structure, this results in a reduction of the ion-electrode distance which is undesirable due to the increase in ion motional heating [23, 24], and the increased chance that stray scattered light from the optical control fields used for cooling and engineered spin-spin interactions induces charging of the electrode surfaces resulting in stray electric fields. For operation of the system, it is also desirable to work with trap frequencies which are high enough to avoid common noise sources in the laboratory, which reduces heating and facilitates laser cooling. For a given electrode structure, the motional frequencies can be increased with a corresponding increase in the applied electrode voltages. However at some point this will be limited by voltage breakdown, and therefore it is beneficial to search for optimal electrode layouts for achieving closely spaced ion

traps while retaining high trap frequencies of the individual micro-traps. We consider here the experimental feasibility to generate such surface-electrode trap layouts with high motional coupling between ions in micro-Penning trap arrays for a given applied voltage. Our focus lies in particular on single layer surface-electrode traps as they offer an open planar structure which facilitates optical access. We note that approaches with two planes of electrodes facing each other might allow improved conditions with regards to spin-spin couplings, but these seem to be more technically challenging [12].

Previous work has described methods for obtaining surface-electrode geometries which maximize the achievable curvature of the pseudo-potential in arrays of r.f. traps for a given trapping site density with distance from the electrode surface  $h$  [10]. The problem reduces to maximizing the quadrupole strength which can be produced at the array of sites, which is the identical problem for the Penning trap arrays. However in the case of r.f. traps this quadrupole potential must be converted into a ponderomotive pseudopotential while maintaining conditions suitable for stable motion, while the Penning trap frequencies are directly dependent on the static quadrupole. The advantage this gives can be evaluated by considering the effect of modulating a static potential  $\Pi$  with curvature tensor  $\Pi^{(2)} \equiv \partial_{\mu} \partial_{\nu} \Pi$ ,  $\nu, \mu = x, y, z$  at a radio-frequency  $\Omega_{RF}$ , creating  $\Pi \cos(\Omega_{RF} t)$ . In the pseudopotential approximation [25], the curvature tensor of the pseudopotential for an ion of mass  $m$  is then

$$\Psi_{RF}^{(2)} = \frac{e}{2m\Omega_{RF}^2} \left[ \Pi^{(2)} \right]^2 \quad (5)$$

at any trap centre. For simplicity we focus on a cylindrically symmetric trap potential defined as

$$\Pi = \frac{\phi_0}{h^2} \left( z^2 - \frac{x^2 + y^2}{2} \right). \quad (6)$$

To compare the strength achievable for the r.f. vs Penning trap, we take the Frobenius norm of the curvature tensor, finding that the magnitudes of the two curvature tensors can be related using the Mathieu parameter  $q_z = -\frac{4e\phi_0}{m\Omega_{RF}^2 h^2}$  as

$$\|\Psi_{RF}^{(2)}\| = \frac{\sqrt{3}}{8} |q_z| \cdot \|\Pi^{(2)}\|. \quad (7)$$

Thus the curvature of the pseudopotential is weaker than that of the corresponding static potential by a factor  $\sqrt{3}|q_z|/8$ . For surface-electrode r.f. traps, stability becomes a concern for  $|q_z| > 0.3$ , corresponding to a reduction factor of around 15. In this case, for a given voltage which is applied to the electrodes, the trap frequency in the r.f. trap is reduced relative to a Penning trap with the same geometry by a factor  $\sqrt{15}$ .

The discussion above makes it clear that the optimization of electrode structures for Penning trap arrays is identical to the case of radio-frequency traps, and thus

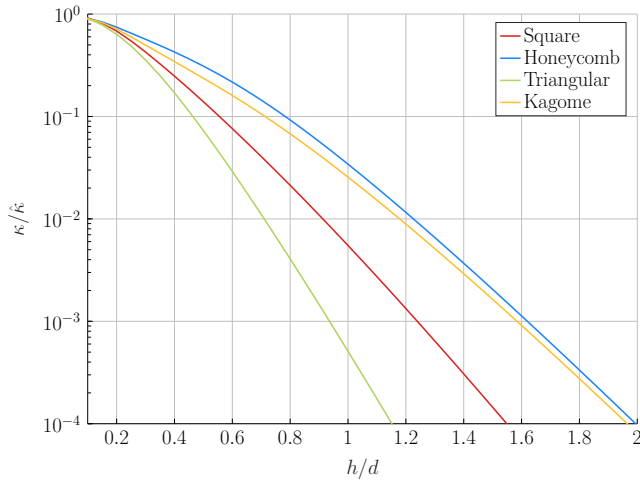


FIG. 2. Dimensionless curvatures  $\kappa$  as functions of the ratio of microtrap height  $h$  to inter-ion spacing  $d$ , for several lattice geometries.

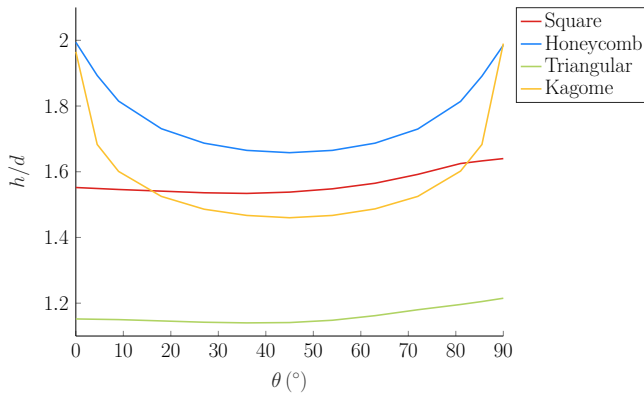


FIG. 3. The value of  $h/d$  for which a dimensionless curvature  $\kappa/\hat{\kappa} = 10^{-4}$  is achieved as a function of the angle of tilt of the trapping axis with respect to the normal of the plane, for several lattice geometries. For the hexagonal and Kagome lattices a strong effect is observed.

produces identical electrode geometries [10, 11]. Similar to the earlier work, we define a dimensionless curvature  $\kappa = \|\Phi^{(2)}\| h^2/V$ , where  $V$  is a fixed voltage applied to part of the electrode plane (the rest being set to zero), and  $h$  is taken to be the distance from the centre of the quadrupole to the nearest trap surface. For the symmetric potential the component of the dimensionless curvature aligned with the magnetic field is  $\hat{\kappa}_z = \hat{\kappa}^{2/3}$ . We then optimize the electrode geometry. Figure 2 shows the the dimensionless curvature of the trap potential achievable for different infinite lattices as a function of the ratio of trap height to inter-ion distance, with the magnetic field directed perpendicular to the plane of the electrodes. The values given are normalized to the dimensionless curvature  $\hat{\kappa} \approx 0.473$  achievable for an optimal surface-electrode point trap [10].

Typical electrode structures in quantum information

experiments can withstand differences in voltages on neighboring electrodes sufficient to achieve  $V = 300$  V [26]. With  $h = 30$   $\mu\text{m}$ ,  $\kappa = 10^{-4}$  then allows to achieve  $\omega_z/(2\pi) = 2.1$  MHz for beryllium ions. Figure 2 indicates that this would allow ions spaced by between 26  $\mu\text{m}$  and 15  $\mu\text{m}$ , with the former corresponding to the triangular lattice and the latter to the Honeycomb and Kagome lattices. The resulting exchange frequencies are between  $11 \text{ kHz} < \Omega_{\text{ex},z}/(2\pi) < 55 \text{ kHz}$ . This is far above heating rates and frequency drift rates observed in traps of a similar size, thus high quality coherent exchange would be expected [27].

The discussion above considers trapping potentials with the confinement direction (and magnetic field) out of the plane of the electrodes. The introduction of a tilt between the electrode plane normal and the magnetic field modifies the geometries of the optimized electrodes and the values of  $\kappa$  which can be achieved. Figure 3 shows the value of  $h/d$  for which a dimensionless curvature  $\kappa/\hat{\kappa} = 10^{-4}$  is achieved as a function of the angle  $\Theta$  between the magnetic field and the normal to the electrode plane. We see that  $\Theta = 90^\circ$  to this plane produces the highest curvatures for all geometries (and thus requires the smallest  $h/d$  to get to  $\kappa/\hat{\kappa} = 10^{-4}$ ), with an additional maximum for  $\Theta = 0^\circ$ . The former allows laser cooling with laser beams in the plane of the electrode surface, the latter does not - previous work in radio-frequency traps indicates that  $\Theta > 8^\circ$  is necessary for robust laser cooling [28]. The change in achievable  $h/d$  for a fixed  $\kappa$  between  $\Theta = 0^\circ$  and  $\Theta = 8^\circ$  is small for the triangular and square lattices, but considerable in the case of the Kagome and Hexagonal lattices.

#### IV. OPERATING CONDITIONS

Within the restrictions of using symmetric quadrupole potentials, there is nevertheless a range of possible choices of  $\omega_c, \omega_z$  which could be used, related to the type of couplings which are desired and the achievable experimental constraints. However these choices are constrained by the fixed dependence of the mode frequencies on these two parameters. As an example which we find interesting from the perspective of engineered tunable-range spin-spin couplings (see section VIII), we consider the challenge of operating a trap with a fixed achievable  $\omega_z$  while desiring that the modes have a large enough splitting that three separated bands of modes occur corresponding to coupled magnetron, modified cyclotron and axial frequencies. As shown in the next section, for an infinite lattice the width of any one band is in the range between 5 and 6 times the exchange frequency for respective mode (in the perturbative limit, the width is  $5.15 \Omega_{\text{ex}}$ ). Figure 4 shows the trap frequencies which can be achieved normalized to the axial frequency  $\omega_z$ . To achieve large mode separations, it appears attractive to work in the regime for which  $\omega_+ > \omega_z$ , which corresponds to  $\omega_c > 3\omega_z/2$ . However note that this implies

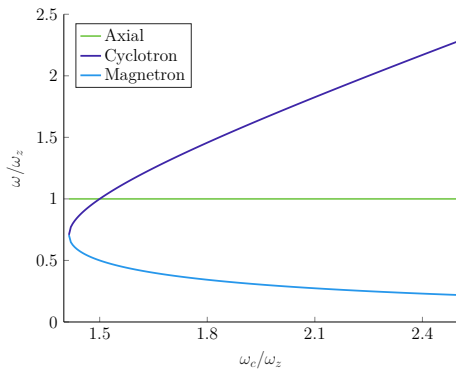


FIG. 4. Frequencies of oscillation of a single ion Penning trap as a function of the cyclotron frequency. All frequencies are given in units of the axial frequency.

that  $\omega_- < \omega_z/2$ . The splitting between the  $\omega_{\pm}$  modes and the axial modes becomes equal in magnitude when  $\omega_c/2 = \omega_z$ , for which  $\omega_- = \omega_z(\sqrt{2}-1)/\sqrt{2} \approx 0.29\omega_z$ . In practice there are good reasons to work with high magnetron frequencies, for example because this would be expected to result in lower heating rates of those modes due to sampling noise at higher frequencies - this may limit the choice of trap parameters.

A second regime of operation could also be used, in which the difference in mode frequencies is significantly below the trap frequencies themselves. For this regime, the axial frequency can be chosen to be the highest frequency of the three, and the modified cyclotron and magnetron modes become closer in frequency. This can be achieved in a narrow regime for which  $3\omega_z/2 > \omega_c > \sqrt{2}\omega_z$ . As  $\omega_c$  is reduced within this range, the difference frequency  $\omega_1$  between the modified cyclotron and magnetron frequencies is reduced. This increases the exchange frequencies for these modes (but also proportionally the heating rate). The maximal separation of modes within this regime is  $0.191\omega_z$ .

## V. NORMAL MODE ANALYSIS

A full analysis of the normal modes of vibration of ions is a prerequisite to understand the methods utilized for laser cooling and implementation of analog quantum simulation. The presence of a magnetic field in Penning traps makes this analysis non-trivial. While the case of a naturally formed two-dimensional ion crystal in a macroscopic Penning trap has been treated before, this involves a transformation to a frame co-rotating with the rigid ion crystal [29]. Here we avoid any such transformation, and derive the normal modes for the general case of ions in an array of micro-Penning traps, assuming only that the equilibrium positions are well defined so that the harmonic approximation for the electric potential can be used and that the magnetic field is uniform over the region explored by each ion. The analysis leads to a gen-

eralization of a well known invariance theorem used for single ions in Penning traps [18, 19].

### A. Classical Treatment

In the classical regime, the normal mode analysis of a finite system of  $N$  trapped ions can be carried out with the help of Lagrangian mechanics. For simplicity, it is assumed that all ions have an identical mass  $m$ , but the analysis can be generalized to systems containing ions with different masses (see Appendix A). In the frame of reference of the laboratory, with no oscillatory fields present, the Lagrangian of the system is given by

$$L = \sum_{j=1}^N \left[ \frac{1}{2} m |\dot{\mathbf{R}}_j|^2 + e \mathbf{A}_j \cdot \dot{\mathbf{R}}_j - e \Phi_j \right], \quad (8)$$

where  $\mathbf{R}_j$  denotes the lab coordinates of ion  $j$ ,  $\mathbf{A}_j = \frac{1}{2}(\mathbf{B} \times \mathbf{R}_j)$  is the vector potential in the symmetric gauge due to the uniform magnetic field  $\mathbf{B} = B_0 \hat{\mathbf{e}}_z$ , and  $\Phi_j$  is the electric potential containing a sum of contributions from the trapping potential for ion  $j$  and the Coulomb interaction potential experienced by this ion due to all others.

The first step in obtaining normal modes is to solve for the equilibrium positions, which we carry out numerically. The second order term in the series expansion of the system Lagrangian about the equilibrium positions dictates the normal mode dynamics of the system near the stable spatial configuration. The equations of motion for the  $3N$ -dimensional vector  $q = [x_1 \dots x_N \ y_1 \dots y_N \ z_1 \dots z_N]^T$  consisting of all the generalized position coordinates can then be deduced as

$$M\ddot{q} - W\dot{q} + \Phi q = 0, \quad (9)$$

where  $M$ ,  $W$  and  $\Phi$  are  $3N \times 3N$  matrices defined as  $M = m \cdot \mathbb{I}_{3N}$ ,  $W_{jk}^{xy} = -W_{jk}^{yx} = eB_0\delta_{jk}$  and  $\Phi_{jk}^{\mu\nu} = \partial q_j^\mu \partial q_k^\nu L$ .  $\Phi$  contains only terms from the static electric potential and the Coulomb interactions. Here the indices  $j, k$  run over the ion numbers 1 to  $N$  while the indices  $\mu, \nu$  run over the Cartesian components  $x, y, z$ . The ‘mass matrix’  $M$  is a real diagonal matrix,  $W$  is a real antisymmetric matrix representing the velocity-dependent forces (often referred to as the ‘damping matrix’), while the ‘stiffness matrix’  $\Phi$  is a real symmetric traceless matrix.

To find the normal modes of motion, we substitute the oscillating trial solution  $q = q_0 e^{-i\omega t}$  which yields the Quadratic Eigenvalue Problem (QEP)

$$[\omega^2 M + \omega(-iW) - \Phi] q_0 = 0, \quad (10)$$

that can be solved for complex eigenvectors  $q_0$  and eigenvalues  $\omega$ . When all eigenvalues are real the motion of all ions is bounded and stable confinement can be achieved. Each of the  $3N$  collective normal modes of motion is thus

characterized by the eigenpair  $\{\omega_\lambda, q_\lambda\}$  and the general solution for the motion can be expressed as

$$q(t) = \text{Re} \left[ \sum_{\lambda=1}^{3N} r_\lambda q_\lambda e^{-i(\omega_\lambda t + \delta_\lambda)} \right] \quad (11)$$

with the amplitude  $r_\lambda$  and phase  $\delta_\lambda$  for each mode  $\lambda$  determined by the initial conditions.

It is important to note that the total energy contained in each mode

$$E_\lambda = \frac{1}{4} r_\lambda^2 (\omega_\lambda^2 q_\lambda^H M q_\lambda + q_\lambda^H \Phi q_\lambda) \quad (12)$$

is not trivially positive, unlike the case of Paul traps. Typically we will observe  $N$  modes dominated by motion along the axial direction and it is convenient to continue calling these modes axial modes in the context of the  $N$  ion array of Penning traps. Each of the axial modes has a positive total mode energy. Similarly there are  $2N$  radial modes out of which  $N$  have each a positive mode energy and  $N$  have each a negative mode energy. We will denote the radial modes with positive sign as cyclotron modes and the ones with negative sign as magnetron modes.

## B. Quantum Mechanical Treatment

The solution for the normal modes of the above described system in the quantum regime involves the formulation of the Hamiltonian in terms of the canonical position and momentum operators and then forming the phonon creation and annihilation operators,  $\hat{a}_\lambda^\dagger$  and  $\hat{a}_\lambda$ , for each mode  $\lambda$  as linear combinations of these operators,

$$\hat{a}_\lambda^\dagger = \sum_{j=1}^{3N} (\alpha_{\lambda j} \hat{p}_j + \beta_{\lambda j} \hat{q}_j), \quad (13)$$

where  $\alpha$  and  $\beta$  are complex numbers. The objective is to find these complex coefficients which allow us to diagonalize the Hamiltonian in terms of the canonical position and momentum operators and then forming the phonon creation and annihilation operators,  $\hat{a}_\lambda^\dagger$  and  $\hat{a}_\lambda$ , for each mode  $\lambda$  as linear combinations of these operators. Combining these requirements, we find that the  $3N$ -dimensional vectors  $\alpha_\lambda$  for each mode  $\lambda$  satisfy the same QEP we had to solve in the classical analysis

$$[\omega^2 M + \omega(-iW) - \Phi] \alpha_\lambda = 0, \quad (14)$$

and we have the relation  $\beta_\lambda = i\omega_\lambda M \alpha_\lambda + \frac{1}{2} W \alpha_\lambda$ . These vectors can then be normalized such that the condition  $[\hat{a}_\lambda, \hat{a}_\lambda^\dagger] = 1$  is fulfilled.

We note that the treatment discussed in this section encompasses both r.f. and Penning traps, and the normal modes for the former under the pseudopotential approximation can be retrieved by choosing the magnetic field strength as zero and adding a suitable pseudopotential term to  $\Phi$ . In this case  $\Phi$  is not trace zero.

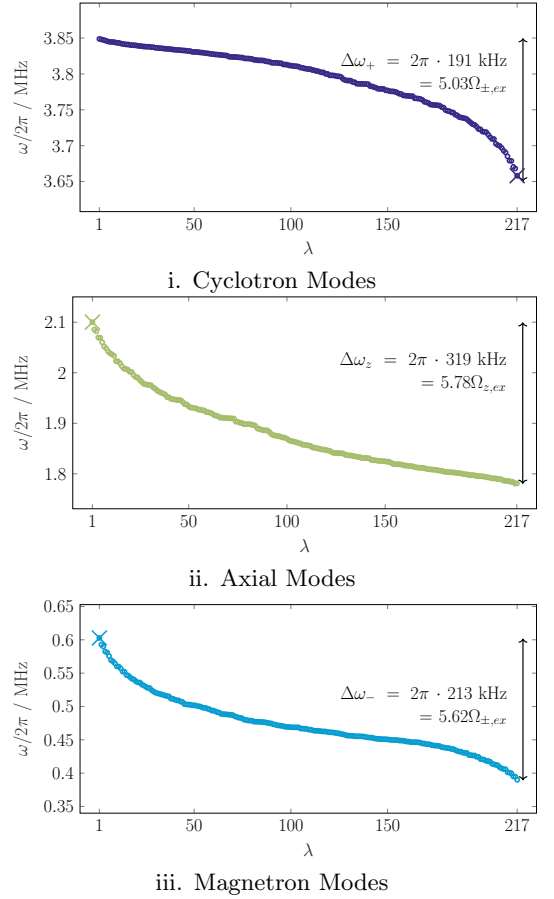


FIG. 5. Frequency spectrum of a 217 ion triangular lattice ( $d = 15 \mu\text{m}$ ) arranged with the tilted configuration ( $\Theta = 20^\circ$ ). Shown here are the cyclotron, axial and magnetron branches of the normal modes. The centre of mass frequency in each mode branch is marked with a cross. The width of each branch is shown in terms of the respective 2-ion exchange frequency through black arrows.

## VI. GENERALIZED INVARIANCE THEOREM

A real trap is imperfect and can suffer from misalignments between the magnetic field and the confining axis of the quadrupole potential, or the trap potential differing from the desired precise form. Including these imperfections in the matrices  $W$  and  $\Phi$  in the QEP encountered in the classical analysis and dividing the equation by  $m$ , we get

$$[\omega^2 \cdot \mathbb{I}_{3N} + \omega(-iW') - \Phi'] q_0 = 0, \quad (15)$$

where we define the matrices  $W' = W/m$  and  $\Phi' = \Phi/m$ . This new QEP can then be linearized by mapping it on to a standard eigenvalue problem while increasing the dimensionality by a factor of two so that we arrive at

$$Av = \omega v, \quad (16)$$



with  $6N$ -dimensional eigenvectors  $v = [q_0 \ \omega q_0]^T$  and  $6N$  eigenvalues  $\omega$  belonging to the  $6N \times 6N$  matrix  $A$

$$A = \begin{bmatrix} \mathbb{O}_{3N} & \mathbb{I}_{3N} \\ \Phi' & iW' \end{bmatrix}. \quad (17)$$

Since  $A^2 v = \omega^2 v$  and the sum of eigenvalues of a matrix is equal to its trace,

$$\sum_{\lambda=1}^{6N} \omega_\lambda^2 = \text{tr}(A^2) = \text{tr}(2\Phi' - W'^2) = -\text{tr}(W'^2). \quad (18)$$

This result will hold for any potential terms added to  $\Phi'$  which exist in free space, since these must be traceless in order to satisfy Laplace's equation (it would not hold for a pseudopotential). While for a single ion only the trapping potentials are present, in the case of a multi-ion system the Coulomb interactions are also contained in this term. Noting that the frequencies come in pairs of positive-negative values in the stable regime we can express this sum in terms of the  $3N$  positive frequencies,

$$\begin{aligned} \sum_{\lambda=1}^{3N} \omega_\lambda^2 &= -\frac{1}{2} \text{tr}(W'^2) \\ &= N\omega_c^2 \end{aligned} \quad (19)$$

where  $\omega_c = eB_0/m$  is the bare cyclotron frequency. This relation between the strength of the magnetic field quantified and the normal mode frequencies of a stable  $N$ -ion system represents a non-trivial generalization of the well known Brown-Gabrielse invariance theorem for a single ion in a Penning trap [18, 19],

$$\omega_+^2 + \omega_-^2 + \omega_z^2 = \omega_c^2. \quad (20)$$

The single-ion invariance theorem is widely used in precision measurement [30]. While we find our generalization to be of interest theoretically, it is unclear whether it has an application to precision measurement, since it seems challenging to measure the frequencies of a large number of modes. A complementary result relating the product of the normal mode frequencies to the curvature of the total electric potential can be derived by taking the determinant of the matrix  $A$  as

$$\prod_{\lambda=1}^{3N} (m\omega_\lambda^2) = |\Phi| \quad (21)$$

The results (19) and (21) further generalize to systems containing ions of different masses (see Appendix C for more details).

## VII. LASER COOLING

Doppler cooling is more complicated in Penning traps as compared to radio-frequency traps due to the fact that

the magnetron modes have a negative total energy. As a consequence the cooling requirements of the magnetron modes are incompatible with those of the axial and cyclotron modes, and no combination of uniform beams can cool all modes of motion simultaneously [31]. One way to combat this is to use a non-uniform beam with intensity gradient but the final temperatures reached for both kinds of radial modes are greater than one would expect from the standard Doppler cooling limit, and the range of motional frequencies that allow for cooling all three kinds of modes is also restricted [31].

An alternative solution which has been realized experimentally [32] is to couple the cyclotron and magnetron modes by applying a weak quadrupolar electric field  $\phi_{\text{ax}}(x^2 - y^2)$  oscillating at the bare cyclotron frequency, in a technique known as axialization [33]. A red-detuned uniform-intensity Doppler cooling laser beam can then simultaneously cool all modes. With the axialization drive the system no longer consists of just electrostatic fields but since the amplitude of such a drive is much lower than the amplitude of the r.f. drive required for Paul traps, the deleterious effects of micromotion are accordingly much smaller. Moreover, this technique works efficiently at all trap frequencies, allowing trapping in regimes not accessible through the use of just inhomogeneous beams.

The derivation of the rate equations of the mode amplitudes of ions due to Doppler cooling in Penning traps in the presence of axialization has no simple analytical solution. Instead, we perform numerical simulations on small numbers of ions in which we numerically integrate the equations of motion of the trapped ion including the axialization potential as well as stochastic momentum kicks which occur with a probability which depends on the Doppler shift between the laser and the ion resonance to simulate photon scattering events. By running the simulation a large number of times, the average classical amplitudes of each mode can be found, which can then be converted to mean quantum phonon occupation numbers. Results of such simulations are shown for laser cooling of a six  $^9\text{Be}^+$  ion honeycomb lattice with lattice constant  $15 \mu\text{m}$  with the confining axes tilted at  $\Theta = 20^\circ$  with respect to the radial plane. Here  $B_0 = 2.5 \text{ T}$  and  $\omega_z = 2\pi \cdot 2.1 \text{ MHz}$ . The uniform laser beam is oriented along the electrode plane so that  $\mathbf{k}_L = \cos \Theta \hat{\mathbf{e}}_x + \sin \Theta \hat{\mathbf{e}}_z$ . The axialization voltage is chosen to be  $\phi_{\text{ax}} = 0.03\phi_0$ . The initial quantum numbers for each mode are chosen within a range close to  $10^4$  quanta. The results show that modes can be cooled with time constants in the range of 0.1-0.2 ms, with final mode occupations in the range of 10-30 quanta. This would be expected for Doppler cooling at these trap frequencies. For coupled ion arrays, it is important that the axialization drive mixes all magnetron modes with the modified cyclotron modes. This implies that the modulation strength must be greater than the width of the relevant spread of frequencies of each set of modes.

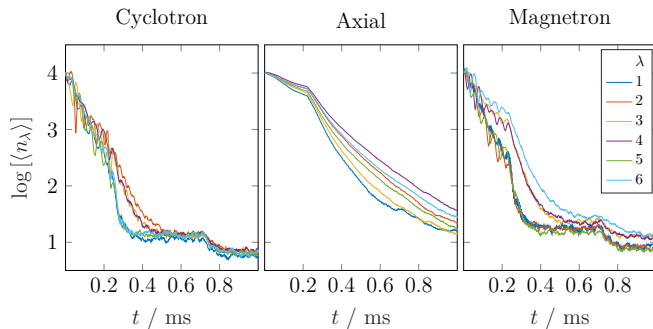


FIG. 6. Laser cooling of a six  ${}^9\text{Be}^+$  ion honeycomb lattice with lattice constant  $15\text{ }\mu\text{m}$  with the confining axes tilted at  $\Theta = 20^\circ$  with respect to the radial plane. Here  $B_0 = 2.5\text{ T}$  and  $\omega_z = 2\pi \cdot 2.1\text{ MHz}$ . The uniform laser beam is oriented along the electrode plane so that  $\mathbf{k}_L = \cos\Theta\hat{\mathbf{e}}_x + \sin\Theta\hat{\mathbf{e}}_z$ . The axialization voltage is chosen to be  $\phi_{\text{ax}} = 0.03\phi_0$ . The initial quantum numbers for each mode are close to  $10^4$  quanta.

### VIII. SPIN-SPIN INTERACTIONS FOR THE ISING MODEL

We now examine the possibility of implementing spin-spin couplings of the form relevant to studying models such as the transverse Ising model [34], which has been a common target of quantum simulation experiments using trapped ions. An effective spin-spin interaction can be generated based on standard techniques developed in the trapped-ion quantum computing community to implement multi-qubit gates [35–38]. These methods rely on the application of forces that depend on the internal (pseudo)spin-state of the ions. For instance, two laser beams off-resonant with respect to the internal transition and with a frequency difference  $\mu_R$  and wave-vector difference  $\mathbf{k}_R$  between each other create a traveling-wave interference pattern at the ions. Each ion experiences a state-dependent optical dipole force (ODF) that oscillates at the frequency  $\mu_R$ . To simplify the algebra, we assume that the two relevant states of the ions are spin-half ground states with no hyperfine structure [39]. In this case, it is possible to generate an ODF that is equal in magnitude but opposite in sign for the two internal states which can be considered as eigenstates of the Pauli operator,  $\hat{\sigma}^z$ . For small coherent displacements of the ions from their equilibrium positions we can use the Lamb-Dicke approximation and keep only resonant terms, resulting in the ODF interaction Hamiltonian

$$\hat{H}_{\text{ODF}} \approx \sum_{j=1}^N E_O \mathbf{k}_R \cdot \mathbf{r}_j \sin(\phi_j - \mu_R t) \hat{\sigma}_j^z \quad (22)$$

where  $E_O$  can be computed using the intensities, frequencies and polarizations of the lasers and the matrix elements of the internal transition of the ions, while the ion dependent phase is given by  $\phi_j = \mathbf{k}_R \cdot \mathbf{R}_{j0}$ . A simi-

lar Hamiltonian can be achieved in a rotated spin basis ( $\hat{\sigma}^x, \hat{\sigma}^y$ ) by driving both red and blue motional sidebands of the spin-flip transition simultaneously [37]. Given the periodic arrangement of ions, we can ensure that this phase is the same for all ions using certain laser beam configurations. In what follows, we assume that this condition is met for the sake of simplicity (see Appendix D for a more general treatment).

The time evolution operator associated with  $\hat{H}_{\text{ODF}}$  can be calculated by carrying out a Magnus expansion in the Interaction Picture, and for the given ODF interaction this yields two terms. The first term describes periodic spin-motion entanglement generated by the ODF. Quantum simulation experiments typically work in the regime in which this entanglement is negligible and can therefore be adiabatically eliminated [5]. The second term describes an effective Ising-like spin Hamiltonian

$$\hat{H}_{\text{SPIN}} = \sum_{jj'} J_{jj'}(t) \hat{\sigma}_j^z \hat{\sigma}_{j'}^z, \quad (23)$$

with the static part of the spin-spin interactions  $J_{jj'}(t)$  given by

$$J_{jj'}^0 = \frac{E_O^2}{2\hbar} \sum_{\lambda} \frac{\omega_{\lambda}}{\mu_R^2 - \omega_{\lambda}^2} \text{Re}(\eta_{\lambda j}^* \eta_{\lambda j'}) \quad (24)$$

Here we have defined the Lamb-Dicke parameters in a slightly unconventional manner as  $\eta_{\lambda j} = \sum_{\nu=x,y,z} k_R^{\nu} \rho_{\lambda 0} \gamma_{\lambda j \nu}$ , with  $\rho_{\lambda 0}$  being the spread of the zero-point wavefunction of mode  $\lambda$  and  $\gamma$  is the corresponding eigenvector normalized to 1. For an r.f. trap this definition reduces to the standard form of the Lamb-Dicke parameter [40].

An interesting aspect of the simulation of the Ising model using trapped ions is the possibility to engineer spin-coupling terms which follow a power-law scaling with the inter-ion separation  $|J_{jj'}| \propto 1/|R_{jj'0}|^a$ , with  $a$  dictated by the experimental detunings [6]. However, such tunable-range interactions are possible only with certain mode structure, in which the center-of-mass (COM) mode has the highest (lowest) frequency in a given band, and the state-dependent force is tuned to a higher (lower) frequency than this mode. In previous experiments with bulk crystals this situation is naturally satisfied, whereas it is not always satisfied in the trap arrays which we consider in this paper. In the following, we trace the importance of the normal mode structure in the determination of the effective spin-spin interactions that can be engineered for a given system of ions.

We first consider the case when the magnetic field is aligned normal to the plane in which the ions lie. With such an orientation the axial motion is decoupled from the radial motion and the COM mode sits at the highest frequency in the axial band. With a wave-vector difference  $\mathbf{k}_R = k_R \hat{\mathbf{e}}_z$ , only the axial modes are excited. By tuning the ODF to the blue of the axial branch variable range spin-spin couplings can be engineered with the range of interaction shortening from infinite range



( $a = 0$ ) to dipole-dipole type ( $a = 3$ ) as  $(\mu_R - \omega_z)$  is increased. Since all coupling terms are positive, this allows to simulate an antiferromagnetic Ising Hamiltonian. Experiments carried so far using both r.f. traps (for eg. Ref. [7]) and Penning traps (for eg. Ref. [6]) are based on this simplification. Conversely, a tunable-range ferromagnetic Ising model can be simulated by aligning  $\mathbf{k}_R$  along the radial plane and tuning the ODF to the red (blue) of the cyclotron (magnetron) branches. This is possible since the cyclotron (magnetron) COM mode is the lowest (highest) in its branch. The coupling terms for the magnetron branch are negative since the magnetron motion represents an inverted harmonic oscillator.

One of the challenges for realizing a setup with the magnetic field normal to the plane is that it is difficult to cool the axial motion or generate an ODF along the axis using lasers directed parallel to the surface of the chip, or equivalently, the plane where the ions sit. While these problems can be countered by using in-chip waveguides [41], we rather attempt to see how well the behavior described above holds when the magnetic field is tilted at an angle  $\Theta$  with respect to the normal of the lattice plane. The crucial factor here is the position of the COM mode within the branch being excited by the ODF. For the trap settings and lattice considered here, this occurs for  $0^\circ \leq \Theta \lesssim 43^\circ$ .

For the case of  $\Theta = 90^\circ$ , that is, when the magnetic field is along the plane, a suitably oriented in-plane laser beam can cool all motional modes. However all three COM modes lie away from the extrema of their respective branches, making it hard to implement variable range spin-spin interactions by tuning  $\mu_R$  alone. With such a mode structure, detuning  $\mu_R$  in either direction from any of the three COM modes does not reveal a well-defined power law decay and the coupling terms have different signs depending on the angle of the inter-ion vector. A histogram plot in figure 8 shows this behavior. The same is expected more generally whenever  $\mu_R$  lies in the middle of the branch of modes used. More complicated methods could make it possible to emulate a tunable-range Ising model with such geometric arrangement of micro-traps [42], but we do not consider this here. At large detunings of the ODF from a given branch, dipole-dipole couplings can be realized with a distance scaling  $|J_{jj'}| \propto 1/|R_{jj'0}|^3$  but the sign of the coupling term between any given pair of spins will be determined mostly by their relative phase in the mode closest to the chosen value of  $\mu_R$ . This frustration in sign might allow for the study of disordered spin dynamics in poorly understood systems such as quantum spin glasses [43]. The same behavior could also be effected by tuning within any phonon branch although the emergence of any power law scaling is not expected, except for the case when the ODF is tuned close to the COM mode, leading to infinite range behavior ( $a = 0$ ).

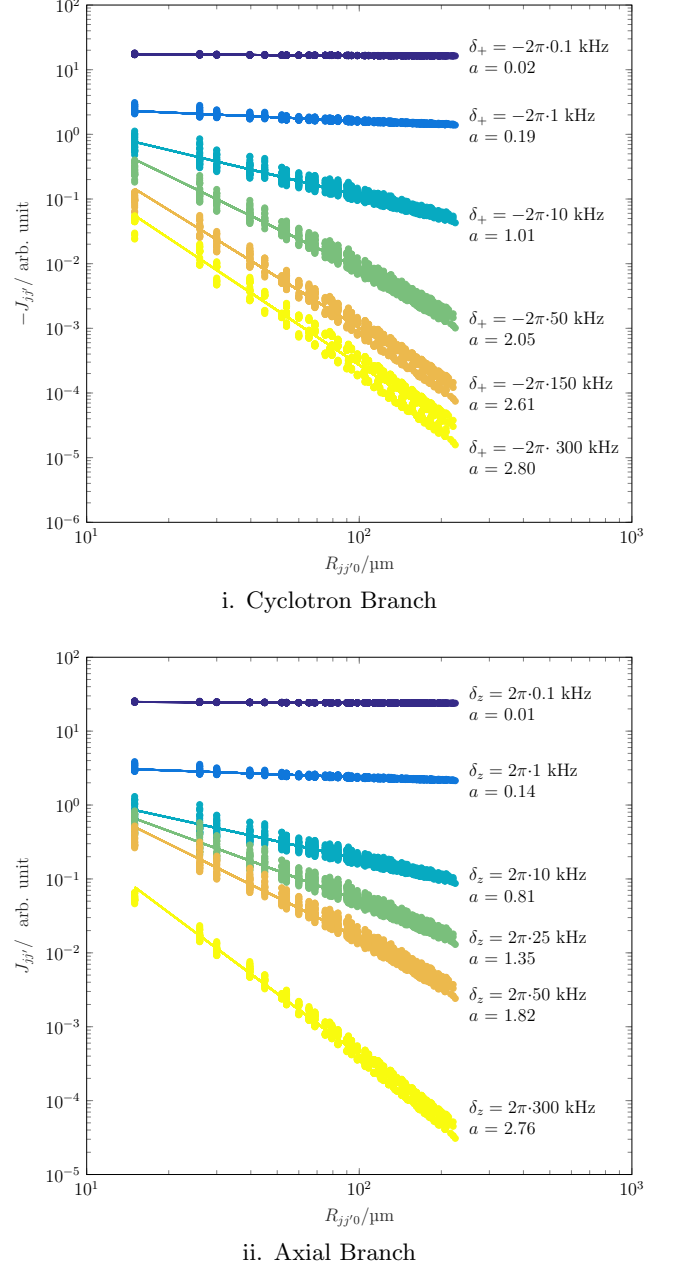


FIG. 7. Spin-spin coupling terms generated with an optical dipole force for a 217 ion triangular lattice ( $d = 15 \mu\text{m}$ ) arranged with the tilted geometry ( $\Theta = 20^\circ$ ). The ODF can be created by two laser beams along the plane of the electrodes so that the difference wave vector is given by  $\mathbf{k}_R = k_R \cos \Theta \hat{\mathbf{e}}_x + k_R \sin \Theta \hat{\mathbf{e}}_z$ . When the beatnote frequency  $\mu_R$  lies to the red of the cyclotron branch, all couplings are negative and a ferromagnetic Ising interaction can be engineered. These couplings follow an approximate power law decay  $|J_{jj'}| \propto 1/|R_{jj'0}|^a$  and the exponent  $a$  increases with increasing magnitude of  $\delta_+ = \mu_R - \omega_+$ . Similar tunable ferromagnetic couplings can be achieved by tuning to the blue of the magnetron COM mode. For the radial modes, lasers parallel to the electrode plane can also be used to create a wavevector difference along the  $\hat{y}$ -axis. When  $\mu_R$  is increasingly tuned away from the axial branch so that  $\delta_z = \mu_R - \omega_z$  increases, all couplings are positive and hence variable range antiferromagnetic Ising like interactions can be generated with  $a$  going from 0 to 3. The strength of these couplings is limited by the angle of tilt  $\Theta$ . Use of laserless methods could eliminate this restriction

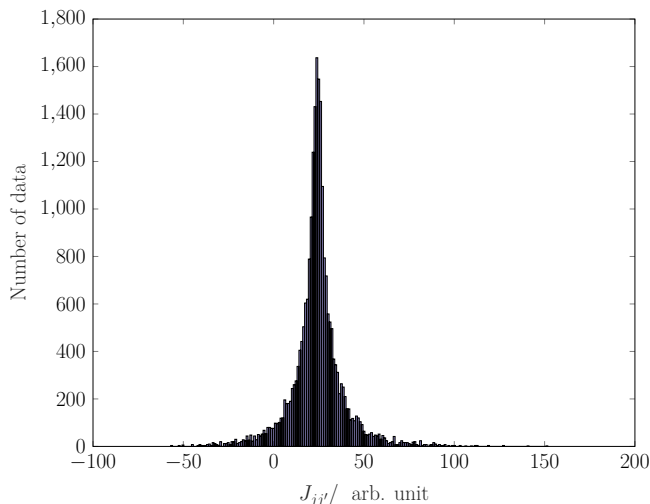


FIG. 8. Histogram plots for spin-spin coupling terms when the beat note frequency  $\mu_R$  is tuned slightly away from the COM frequency of the axial branch. Here  $\mu_R - \omega_z = 2\pi \cdot 0.1$  kHz

## IX. SCALING

The lack of need to drive radio-frequency potentials in the ion trap chip beyond the modest frequencies and voltages required for axialization provides a new perspective for scaling up trapped ion arrays. Many groups currently operate chip traps which are of area between  $1 \text{ mm}^2$  and  $1 \text{ cm}^2$ . For an inter-ion spacing of  $20 \text{ }\mu\text{m}$  on a square lattice, the latter could be used to trap 250,000 ions! This is something which is not currently conceivable with r.f. traps due to a number of factors. Connecting multiple radio-frequency electrodes would involve increased capacitance, which for high voltages implies a corresponding increase in power dissipation. Stray electric fields in Paul traps lead to misalignment of the radio-frequency and static quadrupole potentials, resulting in undesirable micromotion which affects the interaction of the ion with laser fields. In Penning traps, these move the center of the trap, but do not produce any other undesirable effect. Recent evidence suggests that heating may be linked to

processes driven by the radio-frequency drive in Paul traps, which gives hope that anomalous heating could be significantly reduced in the systems proposed here [44]. Co-wiring of one million electrodes is within the capabilities of fabrication based on commercial Complementary-Metal-on-Silicon processes which have previously been used for surface traps [45], while the possibility to also integrate optics [41] may also relax constraints on optical beam delivery.

## X. CONCLUSIONS

The current paper establishes the possibility of using Penning trap arrays for many-body quantum simulations using trapped-ions. While we consider only motional modes and the possibility to realize tunable-range spin-spin interactions, different engineered couplings could be used to access a wide range of possibilities which have been previously discussed in the context of other systems, including but not limited to spin-boson systems [21], dissipative simulations [46], and engineered topology [47]. We note however that the static arrays considered here are only one way of scaling more general trapped-ion quantum information setups. Breaking the lattice down into smaller units would allow small ion separations to be achieved with significantly reduced voltages [8]. This could be combined with the use of dynamic changes to the trapping potentials to extend the reach of Penning microtrap arrays into scalable architectures for quantum computing [25, 48, 49]. Here they hold the considerable advantage that there is no need to separate regions for quantum gates from specialized junction regions where 2-dimensional transport occur [50, 51]. The magnetic field supplies 3-dimensional confinement anywhere that a static quadrupole can be placed, thus re-organization of the potential landscape in 3-dimensions would allow 3-dimensional movement of ions at any point above the trap surface. This, along with the lack of high voltage radio-frequency potentials, would remove multiple constraints on scaling trapped-ion quantum computing, and pave the way to useful quantum computers.

- 
- [1] R. P. Feynman, International Journal of Theoretical Physics **21**, 467 (1982).
  - [2] T. Häner and D. S. Steiger, in *Proceedings of the International Conference for High Performance Computing, Networking, Storage and Analysis*, SC '17 (ACM, New York, NY, USA, 2017) pp. 33:1–33:10.
  - [3] I. Georgescu, “Foundations of quantum mechanics,” (2014).
  - [4] T. Schaetz, C. R. Monroe, and T. Esslinger, New Journal of Physics **15**, 085009 (2013).
  - [5] R. Blatt and C. F. Roos, Nature Physics **8**, 277 (2012).
  - [6] J. W. Britton, B. C. Sawyer, C.-C. J. W. A. C. Keith, J. K. Freericks, H. Uys, M. J. Biercuk, and J. J. Bollinger, Nature **484**, 489 (2012).
  - [7] J. Zhang, G. Pagano, P. W. Hess, A. Kyprianidis, P. Becker, H. Kaplan, A. V. Gorshkov, Z.-X. Gong, and C. Monroe, Nature **551**, 601 (2017).
  - [8] M. Mielenz, H. Kalis, M. Wittmer, F. Hakeberg, U. Warring, R. Schmied, M. Blain, P. Maunz, D. L. Moehring, D. Leibfried, *et al.*, Nature communications **7**, ncomms11839 (2016).
  - [9] A. C. Wilson, Y. Colombe, K. R. Brown, E. Knill, D. Leibfried, and D. J. Wineland, Nature **512**, 57 (2014).

- [10] R. Schmied, J. H. Wesenberg, and D. Leibfried, *Phys. Rev. Lett.* **102**, 233002 (2009).
- [11] R. Schmied, J. H. Wesenberg, and D. Leibfried, *New Journal of Physics* **13**, 115011 (2011).
- [12] F. N. Krauth, J. Alonso, and J. P. Home, *Journal of Physics B: Atomic, Molecular and Optical Physics* **48**, 015001 (2015).
- [13] D. J. Berkeland, J. D. Miller, J. C. Bergquist, W. M. Itano, and D. J. Wineland, *Journal of Applied Physics* **83**, 5025 (1998).
- [14] G. Ciaramicoli, I. Marzoli, and P. Tombesi, *Phys. Rev. Lett.* **91**, 017901 (2003).
- [15] S. Stahl, F. Galve, J. Alonso, S. Djekic, W. Quint, T. Valenzuela, J. Verdú, M. Vogel, and G. Werth, *The European Physical Journal D-Atomic, Molecular, Optical and Plasma Physics* **32**, 139 (2005).
- [16] P. Bushev, S. Stahl, R. Natali, G. Marx, E. Stachowska, G. Werth, M. Hellwig, and F. Schmidt-Kaler, *The European Physical Journal D* **50**, 97 (2008).
- [17] J. Goldman and G. Gabrielse, *Physical Review A* **81**, 052335 (2010).
- [18] L. S. Brown and G. Gabrielse, *Phys. Rev. A* **25**, 2423 (1982).
- [19] L. S. Brown and G. Gabrielse, *Reviews of Modern Physics* **58**, 233 (1986).
- [20] R. Hendricks, E. Phillips, D. Segal, and R. Thompson, *Journal of Physics B: Atomic, Molecular and Optical Physics* **41**, 035301 (2008).
- [21] D. Porras, F. Marquardt, J. von Delft, and J. I. Cirac, *Phys. Rev. A* **78**, 010101(R) (2008).
- [22] Q. A. Turchette, D. Kielpinski, B. E. King, D. Leibfried, D. M. Meekhof, C. J. Myatt, M. A. Rowe, C. A. Sackett, C. S. Wood, W. M. Itano, C. Monroe, and D. J. Wineland, *Phys. Rev. A* **61**, 063418 (2000).
- [23] L. Deslauriers, S. Olmschenk, D. Stick, W. K. Hensinger, J. Sterk, and C. Monroe, *Phys. Rev. Lett.* **97**, 103007 (2006).
- [24] M. Brownnutt, M. Kumph, P. Rabl, and R. Blatt, *Rev. Mod. Phys.* **87**, 1419 (2015).
- [25] D. J. Wineland, C. Monroe, W. M. Itano, D. Leibfried, B. E. King, and D. M. Meekhof, *J. Res. Natl. Inst. Stand. Technol.* **103**, 259 (1998).
- [26] R. Sterling, M. Hughes, C. Mellor, and W. Hensinger, *Applied Physics Letters* **103**, 143504 (2013).
- [27] K. R. Brown, C. Ospelkaus, Y. Colombe, A. C. Wilson, D. Leibfried, and D. J. Wineland, *Nature* **471**, 196 (2011).
- [28] F. Lindenefser, M. Marinelli, V. Negnevitsky, S. Ragg, and J. P. Home, *New Journal of Physics* **19**, 063041 (2017).
- [29] C.-C. J. Wang, A. C. Keith, and J. K. Freericks, *Phys. Rev. A* **87**, 013422 (2013).
- [30] G. Gabrielse, *Phys. Rev. Lett.* **102**, 172501 (2009).
- [31] W. M. Itano and D. J. Wineland, *Phys. Rev. A* **25**, 35 (1982).
- [32] H. Powell, D. Segal, and R. Thompson, *Physical review letters* **89**, 093003 (2002).
- [33] R. C. Thompson and J. Papadimitriou, *Journal of Physics B: Atomic, Molecular and Optical Physics* **33**, 3393 (2000).
- [34] E. Ising, *Zeitschrift für Physik* **31**, 253 (1925).
- [35] D. Leibfried, B. DeMarco, V. Meyer, D. Lucas, M. Barrett, J. Britton, W. M. Itano, B. Jelenkovic, C. Langer, T. Rosenband, and D. J. Wineland, *Nature* **422**, 412 (2003).
- [36] K. Mølmer and A. Sørensen, *Phys. Rev. Lett.* **82**, 1835 (1999).
- [37] C. F. Roos, T. Monz, K. Kim, M. Riebe, H. Häffner, D. F. V. James, and R. Blatt, *Phys. Rev. A* **77**, 040302 (2008).
- [38] K. Kim, M.-S. Chang, R. Islam, S. Korenblit, L.-M. Duan, and C. Monroe, *Phys. Rev. Lett.* **103**, 120502 (2009).
- [39] J. P. Home, M. J. McDonnell, D. M. Lucas, G. Imreh, B. C. Keitch, D. J. Szwer, N. R. Thomas, D. N. Stacey, and A. M. Steane, *New J. Phys.* **8**, 188 (2006).
- [40] J. P. Home, D. Hanneke, J. D. Jost, D. I. Leibfried, and D. J. Wineland, *New J. Phys.* **13**, 073026 (2011).
- [41] K. K. Mehta, C. D. Bruzewicz, R. McConnell, R. J. Ram, J. M. Sage, and J. Chiaverini, *Nature Nanotechnology* **11**, 1066 (2016).
- [42] S. Korenblit, D. Kafri, W. C. Campbell, R. Islam, E. E. Edwards, Z.-X. Gong, G.-D. Lin, L.-M. Duan, J. Kim, K. Kim, and C. Monroe, *New J. Phys.* (2012).
- [43] S. F. Edwards and P. W. Anderson, *Journal of Physics F: Metal Physics* **5**, 965 (1975).
- [44] D. A. Hite, K. S. McKay, S. Kotler, D. Leibfried, D. J. Wineland, and D. P. Pappas, *MRS Advances* **2**, 2189 (2017).
- [45] K. K. Mehta, A. Eltony, C. Bruzewicz, I. Chuang, R. Ram, J. Sage, and J. Chiaverini, *Applied Physics Letters* **105**, 044103 (2014).
- [46] J. T. Barreiro, M. Müller, P. Schindler, D. Nigg, T. Monz, M. Chwalla, M. Hennrich, C. F. Roos, P. Zoller, and R. Blatt, *Nature* **470**, 486 (2011).
- [47] A. Bermudez, T. Schaetz, and D. Porras, *Physical review letters* **107**, 150501 (2011).
- [48] D. Kielpinski, C. Monroe, and D. Wineland, *Nature* **417**, 709 (2002).
- [49] M. Hellwig, A. Bautista-Salvador, K. Singer, G. Werth, and F. Schmidt-Kaler, *New Journal of Physics* **12**, 065019 (2010).
- [50] R. B. Blakestad, C. Ospelkaus, A. P. VanDevender, J. M. Amini, J. Britton, D. Leibfried, and D. J. Wineland, *Phys. Rev. Lett.* **102**, 153002 (2009).
- [51] G. Shu, G. Vittorini, A. Buikema, C. S. Nichols, C. Volin, D. Stick, and K. R. Brown, *Phys. Rev. A* **89**, 062308 (2014).

## Appendix A: Normal modes: classical description

We consider a system of  $N$  micro-Penning traps containing a single ion each (with charge  $+e$ ) arranged arbitrarily in space. The Coulomb interaction between ions leads to a coupling between their motional states, resulting in  $3N$  collective normal modes of motion.

### Lagrangian Formulation

Let the quadrupole center  $j$  and the position of the ion  $j$  in the reference frame of the lab be defined by the coordinates  $\mathbf{D}_j$  and  $\mathbf{R}_j$  respectively. Then the local coordinates of the ion  $j$  with respect to this quadrupole

center are given by the vector  $\bar{\mathbf{r}}_j = \mathbf{R}_j - \mathbf{D}_j$ .

The trapping electrodes create a static quadrupole electric potential centered at each site  $j$  and this potential can be written in terms of the local coordinates as  $\phi_j = \sum_{\mu\nu} \phi_{j0}^{\mu\nu} \bar{r}_j^\mu \bar{r}_j^\nu$ , where the indices  $\mu$  and  $\nu$  run over the Cartesian components,  $x$ ,  $y$  and  $z$ .

The electrostatic potential acting on the ion  $j$  due to the Coulomb interaction with other ions is

$$\kappa_j = \sum_{k \neq j} \frac{e}{4\pi\epsilon_0 |\mathbf{R}_j - \mathbf{R}_k|} = k_e e \sum_{k \neq j} \frac{1}{|\mathbf{R}_{jk}|}, \quad (\text{A1})$$

where  $k_e = 1/(4\pi\epsilon_0)$  is the Coulomb constant.

The total electric potential, in the absence of any oscillating fields, is thus given by  $\Phi_j = \phi_j + \kappa_j$ .

A static homogeneous magnetic field  $\mathbf{B} = B_0 \sin \theta \cos \varphi \hat{\mathbf{e}}_x + B_0 \sin \theta \sin \varphi \hat{\mathbf{e}}_y + B_0 \cos \theta \hat{\mathbf{e}}_z$  creates the vector potential  $\mathbf{A}_j$  at the site  $j$ . In the symmetric gauge,  $\mathbf{A}_j = \frac{1}{2}(\mathbf{B} \times \mathbf{R}_j)$ .

In the laboratory frame of reference, the total Lagrangian of the system is then given by

$$L_{\text{tot}} = \sum_{j=1}^N \left\{ \frac{1}{2} m_j |\dot{\mathbf{R}}_j|^2 + e \mathbf{A}_j \cdot \dot{\mathbf{R}}_j - e \Phi_j \right\}, \quad (\text{A2})$$

where  $m_j$  is the mass of the  $j$ th ion.

The normal mode analysis begins by finding the equilibrium configuration of ions  $\{\mathbf{R}_{j0}\}$ , which is determined by the minimum of the total potential energy. By expanding the system Lagrangian about the equilibrium position of each ion in a Taylor series up to second order, we get a Lagrangian in terms of the generalized position vectors  $\mathbf{r}_j = \mathbf{R}_j - \mathbf{R}_{j0}$  which specify the displacement of each ion from its equilibrium point. The second order term in the expansion effectively determines the normal mode dynamics of the system near the stable spatial configuration and is given by

$$L = \sum_{j=1}^N \left\{ \frac{1}{2} m_j |\dot{\mathbf{r}}_j|^2 + \frac{e}{2} (\mathbf{B} \times \mathbf{r}_j) \cdot \dot{\mathbf{r}}_j - e \sum_{\mu\nu} \phi_{j0}^{\mu\nu} r_j^\mu r_j^\nu \right\} - \frac{k_e e^2}{2} \sum_{j=1}^N \sum_{k \neq j}^N \left\{ \sum_{\mu} \frac{3R_{jk0}^{\mu 2} - R_{jk0}^2}{R_{jk0}^5} (r_j^\mu - r_k^\mu)^2 + \sum_{\mu \neq \nu} \frac{3R_{jk0}^\mu R_{jk0}^\nu}{R_{jk0}^5} (r_j^\mu - r_k^\mu)(r_j^\nu - r_k^\nu) \right\}. \quad (\text{A3})$$

We proceed by putting together all the generalized position coordinates into a single  $3N$ -dimensional vector  $q = [x_1 \dots x_N \ y_1 \dots y_N \ z_1 \dots z_N]^T$  and introducing the

$3N \times 3N$  block matrices  $M$ ,  $W$ ,  $V$  and  $K$  constructed in terms of  $N \times N$  sub-matrices as

$$M = \begin{bmatrix} M^{xx} & \mathbb{O}_N & \mathbb{O}_N \\ \mathbb{O}_N & M^{yy} & \mathbb{O}_N \\ \mathbb{O}_N & \mathbb{O}_N & M^{zz} \end{bmatrix}, \quad W = eB_0 \begin{bmatrix} \mathbb{O}_N & \cos \theta \cdot \mathbb{I}_N & -\sin \theta \sin \varphi \cdot \mathbb{I}_N \\ -\cos \theta \cdot \mathbb{I}_N & \mathbb{O}_N & \sin \theta \cos \varphi \cdot \mathbb{I}_N \\ \sin \theta \sin \varphi \cdot \mathbb{I}_N & -\sin \theta \cos \varphi \cdot \mathbb{I}_N & \mathbb{O}_N \end{bmatrix}, \quad (\text{A4})$$

$$V = \begin{bmatrix} V^{xx} & V^{xy} & V^{xz} \\ V^{yx} & V^{yy} & V^{yz} \\ V^{zx} & V^{zy} & V^{zz} \end{bmatrix}, \quad K = \begin{bmatrix} K^{xx} & K^{xy} & K^{xz} \\ K^{yx} & K^{yy} & K^{yz} \\ K^{zx} & K^{zy} & K^{zz} \end{bmatrix}.$$

Here  $\mathbb{I}_N$  and  $\mathbb{O}_N$  represent the  $N \times N$  identity and zero matrices respectively and the components of other sub-matrices are defined as

$$M_{jk}^{\mu\mu} = m_j \delta_{jk} \quad (\text{A5})$$

$$V_{jk}^{\mu\nu} = 2e\phi_{j0}^{\mu\nu} \delta_{jk}, \quad (\text{A6})$$

$$K_{jk}^{\mu\mu} = \begin{cases} -k_e e^2 \sum_{l \neq j} \frac{R_{jl0}^2 - 3R_{jl0}^{\mu 2}}{R_{jl0}^5}, & j = k \\ k_e e^2 \frac{R_{jk0}^2 - 3R_{jk0}^{\mu 2}}{R_{jk0}^5}, & j \neq k \end{cases}, \quad (\text{A7a})$$

$$K_{jk}^{\mu\nu} = \begin{cases} 3k_e e^2 \sum_{l \neq j} \frac{R_{jl0}^\mu R_{jl0}^\nu}{R_{jl0}^5}, & j = k \\ -3k_e e^2 \frac{R_{jl0}^\mu R_{jk0}^\nu}{R_{jk0}^5}, & j \neq k \end{cases}, \quad \mu \neq \nu, \quad (\text{A7b})$$

where indices  $j$  and  $k$  run from 1 to  $N$  while again the indices  $\mu$  and  $\nu$  refer to the components  $x$ ,  $y$  and  $z$ .

The above definitions together with  $\Phi = V + K$  allow us to write the effective phonon Lagrangian compactly as

$$L = \sum_{j=1}^{3N} \left\{ \frac{1}{2} M_{jj} \dot{q}_j^2 - \frac{1}{2} \sum_{k=1}^{3N} W_{jk} \dot{q}_j q_k - \frac{1}{2} \sum_{k=1}^{3N} \Phi_{jk} q_j q_k \right\}. \quad (\text{A8})$$

It should be clear that  $M$  is a real diagonal matrix while  $W$  is a real antisymmetric matrix. The matrix  $V$  is traceless as a direct consequence of Laplace's equation, while the matrix  $K$  is traceless because the Coulomb forces being internal forces in the system of ions pairwise cancel each other and the total sum equates to zero.  $V$  and  $K$  are also both real and symmetric. As a result  $\Phi = V + K$  is a real symmetric traceless matrix. These properties are useful in determining certain characteristics of the resulting normal mode eigenfrequencies and eigenvectors of the system.

### Equations of Motion

Through the Euler-Lagrange equations,

$$\frac{d}{dt} \left\{ \frac{\partial L}{\partial \dot{q}_j} \right\} = \frac{\partial L}{\partial q_j}, \quad (\text{A9})$$

we can derive from the Lagrangian the equations of motion of our system. The two relevant derivatives are

$$\frac{\partial L}{\partial \dot{q}_j} = M_{jj} \dot{q}_j - \frac{1}{2} \sum_{k=1}^{3N} W_{jk} q_k \quad (\text{A10})$$

and

$$\frac{\partial L}{\partial q_j} = \frac{1}{2} \sum_{k=1}^{3N} W_{jk} \dot{q}_k - \sum_{k=1}^{3N} \Phi_{jk} q_k, \quad (\text{A11})$$

which we can combine to get

$$M_{jj} \ddot{q}_j - \sum_{k=1}^{3N} W_{jk} \dot{q}_k + \sum_{k=1}^{3N} \Phi_{jk} q_k = 0. \quad (\text{A12})$$

In vector form, we can then see that the equations of motion can be written as

$$M \ddot{q} - W \dot{q} + \Phi q = 0. \quad (\text{A13})$$

To find the normal modes of motion, we substitute the oscillating trial solution  $q = q_0 e^{-i\omega t}$  which yields the QEP

$$[\omega^2(M + \omega(-iW) - \Phi)q_0 = 0, \quad (\text{A14})$$

that can be solved for complex eigenvectors  $q_0$  and eigenvalues  $\omega$ , which in general can be complex. The set of eigenvalues  $\{\omega_\lambda\}$  are the normal mode frequencies while the corresponding normalized eigenvectors  $\{q_\lambda\}$  give us the normal mode coordinates.

The general solution can be written as

$$q(t) = \sum_{\lambda=1}^{3N} \rho_\lambda q_\lambda e^{-i\omega_\lambda t}, \quad (\text{A15})$$

where  $\rho_\lambda$  are complex scalars. The motion of the ions in terms of the normal modes can then be retrieved as

$$r(t) = \text{Re}(q(t)) = \frac{1}{2} \sum_{\lambda=1}^{3N} (\rho_\lambda q_\lambda e^{-i\omega_\lambda t} + \rho_\lambda^* q_\lambda^* e^{i\omega_\lambda t}). \quad (\text{A16})$$

For real frequencies, the collective motion is bounded and hence all ions are confined.

### Appendix B: Normal modes: quantum mechanical description

From the Lagrangian of the system we can identify canonical conjugate variables to formulate our Hamiltonian. The generalized momentum corresponding to the generalized position  $q_j$  is given by  $p_j = \frac{\partial L}{\partial \dot{q}_j}$ . The classical Hamiltonian of the system is then

$$\begin{aligned} H &= \sum_{j=1}^{3N} \dot{q}_j p_j - L \\ &= \sum_{j=1}^{3N} \left\{ \frac{1}{2} M_{jj} \dot{q}_j^2 + \frac{1}{2} \sum_{k=1}^{3N} \Phi_{jk} q_j q_k \right\}. \end{aligned} \quad (\text{B1})$$

Quantizing the generalized coordinates as operators satisfying the standard commutation relations

$$[\hat{q}_j, \hat{q}_k] = 0, \quad [\hat{p}_j, \hat{p}_k] = 0, \quad [\hat{q}_j, \hat{p}_k] = i\hbar \delta_{jk}, \quad (\text{B2})$$

we can formulate the quantum mechanical Hamiltonian of the system as

$$\hat{H} = \sum_{j=1}^{3N} \left\{ \frac{\hat{p}_j^2}{2M_{jj}} + \frac{1}{4M_{jj}} \sum_{k=1}^{3N} W_{jk} \hat{p}_j \hat{q}_k - \sum_{k=1}^{3N} \frac{W_{jk}}{4M_{kk}} \hat{q}_j \hat{p}_k - \frac{1}{8} \sum_{k=1}^{3N} T_{jk} \hat{q}_j \hat{q}_k + \frac{1}{2} \sum_{k=1}^{3N} \Phi_{jk} \hat{q}_j \hat{q}_k \right\}. \quad (\text{B3})$$

where  $T = WM^{-1}W$  is a real symmetric matrix. To diagonalize the Hamiltonian in the second quantized form  $\hat{H} = \sum_{\lambda=1}^{3N} \hbar \omega_\lambda (\hat{a}_\lambda^\dagger \hat{a}_\lambda + \frac{1}{2})$ , we form the phonon

creation and annihilation operators,  $\hat{a}_\lambda^\dagger$  and  $\hat{a}_\lambda$ , for the mode  $\lambda$  as linear combinations of the generalized position

and momentum operators,

$$\hat{a}_\lambda^\dagger = \sum_{k=1}^{3N} (\alpha_{\lambda k} \hat{p}_k + \beta_{\lambda k} \hat{q}_k), \quad (\text{B4})$$

$$\hat{a}_\lambda = \sum_{k=1}^{3N} (\alpha_{\lambda k}^* \hat{p}_k + \beta_{\lambda k}^* \hat{q}_k), \quad (\text{B5})$$

where  $\alpha_{\lambda k}$  and  $\beta_{\lambda k}$  are complex numbers. For the commutation relation  $[\hat{a}_\lambda, \hat{a}_{\lambda'}^\dagger] = \delta_{\lambda\lambda'}$  to hold, the Hamiltonian must satisfy the commutation relation

$$[\hat{H}, \hat{a}_\lambda^\dagger] = \hbar\omega_\lambda \hat{a}_\lambda^\dagger. \quad (\text{B6})$$

This commutator can be calculated by substituting  $\hat{H}$  and  $\hat{a}_\lambda^\dagger$  in terms of the canonical variables and comparing the coefficients of  $\hat{p}_l$  and  $\hat{q}_l$  in  $[\hat{H}, \hat{a}_\lambda^\dagger] = \hbar\omega_\lambda \sum_{l=1}^{3N} (\alpha_{\lambda l} \hat{p}_l + \beta_{\lambda l} \hat{q}_l)$  yields the following set of coupled equations

$$-i \frac{\beta_{\lambda l}}{M_{ll}} + \frac{i}{2} \sum_{m=1}^N \frac{W_{lm}}{M_{ll}} \alpha_{\lambda m} = \omega_\lambda \alpha_{\lambda l}, \quad (\text{B7a})$$

$$i \sum_{m=1}^N \left\{ \frac{W_{lm}}{2M_{mm}} \beta_{\lambda m} - \frac{T_{lm}}{4} \alpha_{\lambda m} + \Phi_{lm} \alpha_{\lambda m} \right\} = \omega_\lambda \beta_{\lambda l}. \quad (\text{B7b})$$

These can be written more succinctly in vector form as

$$-iM^{-1}\beta_\lambda + \frac{i}{2}M^{-1}W\alpha_\lambda = \omega_\lambda \alpha_\lambda, \quad (\text{B8a})$$

$$\frac{i}{2}WM^{-1}\beta_\lambda - \frac{i}{4}T\alpha_\lambda + i\Phi\alpha_\lambda = \omega_\lambda \beta_\lambda. \quad (\text{B8b})$$

On eliminating  $\beta_\lambda$  using  $\beta_\lambda = i\omega_\lambda M\alpha_\lambda + \frac{1}{2}W\alpha_\lambda$ , we then see that

$$\omega_\lambda^2 M\alpha_\lambda - i\omega_\lambda W\alpha_\lambda - \Phi\alpha_\lambda = 0, \quad (\text{B9})$$

which is the same QEP encountered in the classical analysis in Appendix A. The QEP yields  $6N$  eigenvectors and  $6N$  eigenvalues.  $3N$  eigenvectors will be used to form the creation operators while the other  $3N$  eigenvectors to form the annihilation operators. We note that if the pair  $(\nu_\lambda, u_\lambda)$  satisfies the QEP then the pair  $(-\nu_\lambda, u_\lambda^*)$  also satisfies the QEP. Thus the total set of  $6N$  eigenpairs

$$S = \{(\nu_\lambda, u_\lambda), \quad | \quad \nu_\lambda^2 M u_\lambda - i\nu_\lambda W u_\lambda - \Phi u_\lambda = 0\} \quad (\text{B10})$$

for  $\lambda$  running over 1 to  $6N$  can be divided into two equally sized subsets depending on the signs of the eigenvalues:

$$\begin{aligned} S_+ &:= \{(\nu_\lambda, u_\lambda) \quad | \quad (\nu_\lambda, u_\lambda) \in S, \quad \nu_\lambda > 0\}, \\ S_- &:= \{(-\nu_\lambda, u_\lambda^*) \quad | \quad (\nu_\lambda, u_\lambda) \in S, \quad \nu_\lambda > 0\}. \end{aligned} \quad (\text{B11})$$

The index  $\lambda$  now runs from 1 to  $3N$  so that  $\nu_\lambda$  is assumed to be positive from hereon.

Selecting the  $3N$  eigenpairs which form the creation operators effectively means picking the sign of the eigenfrequency (and the corresponding eigenvector) for a given mode  $\lambda$  in  $\hat{H} = \sum_{\lambda=1}^{3N} \hbar\omega_\lambda (\hat{a}_\lambda^\dagger \hat{a}_\lambda + \frac{1}{2})$  and involves fixing the normalization of the eigenvectors  $\alpha_\lambda$  so that  $[\hat{a}_\lambda, \hat{a}_\lambda^\dagger] = 1$ . Explicitly,

$$\begin{aligned} [\hat{a}_\lambda, \hat{a}_\lambda^\dagger] &= i\hbar(\beta_\lambda^H \alpha_\lambda - \alpha_\lambda^H \beta_\lambda) \\ &= \frac{\hbar}{\omega_\lambda} (\omega_\lambda^2 \alpha_\lambda^H M \alpha_\lambda + \alpha_\lambda^H \Phi \alpha_\lambda). \end{aligned} \quad (\text{B12})$$

Substituting  $\alpha_\lambda = c_\lambda \gamma_\lambda$ , where  $\gamma_\lambda$  is normalized to one and  $c_\lambda$  is a complex scalar,

$$[\hat{a}_\lambda, \hat{a}_\lambda^\dagger] = \frac{\hbar|c_\lambda|^2}{\omega_\lambda} \{\omega_\lambda^2 \gamma_\lambda^H M \gamma_\lambda + \gamma_\lambda^H \Phi \gamma_\lambda\}, \quad (\text{B13})$$

which for the condition  $[\hat{a}_\lambda, \hat{a}_\lambda^\dagger] = 1$  yields

$$|c_\lambda|^2 = \frac{\omega_\lambda}{\hbar} \left\{ \frac{1}{\omega_\lambda^2 \gamma_\lambda^H M \gamma_\lambda + \gamma_\lambda^H \Phi \gamma_\lambda} \right\}. \quad (\text{B14})$$

Since  $|c_\lambda|^2$  is non-negative,  $[\hat{a}_\lambda, \hat{a}_\lambda^\dagger] = 1$  only when the quantity  $\omega_\lambda / (\omega_\lambda^2 \gamma_\lambda^H M \gamma_\lambda + \gamma_\lambda^H \Phi \gamma_\lambda)$  is positive. This expression helps us pick out the  $3N$  eigenpairs to form the creation operators

$$(\omega_\lambda, \alpha_\lambda) = \begin{cases} (\nu_\lambda, c_\lambda \gamma_\lambda) & , \nu_\lambda^2 \gamma_\lambda^H M \gamma_\lambda + \gamma_\lambda^H \Phi \gamma_\lambda > 0 \\ (-\nu_\lambda, c_\lambda \gamma_\lambda^*) & , \nu_\lambda^2 \gamma_\lambda^H M \gamma_\lambda + \gamma_\lambda^H \Phi \gamma_\lambda < 0 \end{cases}, \quad (\text{B15})$$

where

$$c_\lambda = \sqrt{\frac{\nu_\lambda}{\hbar|\nu_\lambda^2 \gamma_\lambda^H M \gamma_\lambda + \gamma_\lambda^H \Phi \gamma_\lambda|}} \quad (\text{B16})$$

can without loss of generality be chosen as real. Further, inverting the expressions for the creation and annihilation operators yields the second quantized form of the position and momentum operators,

$$\begin{aligned} \hat{q}_j &= -i\hbar \sum_{\lambda=1}^{3N} (\alpha_{\lambda j}^* \hat{a}_\lambda^\dagger - \alpha_{\lambda j} \hat{a}_\lambda) \\ &= -i\hbar \sum_{\lambda=1}^{3N} c_\lambda (\gamma_{\lambda j}^* \hat{a}_\lambda^\dagger - \gamma_{\lambda j} \hat{a}_\lambda) \end{aligned} \quad (\text{B17})$$

and

$$\hat{p}_j = i\hbar \sum_{\lambda=1}^{3N} (\beta_{\lambda j}^* \hat{a}_\lambda^\dagger - \beta_{\lambda j} \hat{a}_\lambda). \quad (\text{B18})$$

### Appendix C: Trap imperfections

In a real experimental setup, the trapping potential may not be of the idealized form expected from the optimization of the electrode structures, while the magnetic



field could be misaligned with the confining direction of the potential. As long as the imperfections in the electric potential are harmonic and the magnetic field is homogeneous over the entire system, we could employ the general discussion in Appendix A in order to study the normal modes of the imperfect system.

Linearization of the QEP A14 in the first-companion form yields the GEP

$$\begin{bmatrix} \mathbb{O}_{3N} & \mathbb{I}_{3N} \\ \Phi & iW \end{bmatrix} \begin{bmatrix} q_0 \\ \omega q_0 \end{bmatrix} = \omega \begin{bmatrix} \mathbb{I}_{3N} & \mathbb{O}_{3N} \\ \mathbb{O}_{3N} & M \end{bmatrix} \begin{bmatrix} q_0 \\ \omega q_0 \end{bmatrix}. \quad (\text{C1})$$

Inversion of the matrix on the r.h.s. of the above equation leads to a further reduction to the SEP

$$Av = \omega v, \quad (\text{C2})$$

with  $6N$ -dimensional eigenvectors  $v = [q_0 \ \omega q_0]^T$  and  $6N$  eigenvalues  $\omega$  belonging to the  $6N \times 6N$  matrix

$$A = \begin{bmatrix} \mathbb{I}_{3N} & \mathbb{O}_{3N} \\ \mathbb{O}_{3N} & M^{-1} \end{bmatrix} \begin{bmatrix} \mathbb{O}_{3N} & \mathbb{I}_{3N} \\ \Phi & iW \end{bmatrix}. \quad (\text{C3})$$

For the sake of brevity, we define the matrices  $W' = M^{-1}W$  and  $\Phi' = M^{-1}\Phi$ , so that we have

$$A = \begin{bmatrix} \mathbb{O}_{3N} & \mathbb{I}_{3N} \\ \Phi' & iW' \end{bmatrix} \quad (\text{C4})$$

and

$$A^2 = \begin{bmatrix} \Phi' & iW' \\ iW'\Phi' & \Phi' - W'^2 \end{bmatrix}. \quad (\text{C5})$$

Since  $A^2 v = \omega^2 v$  and the sum of eigenvalues of a matrix is equal to its trace,

$$\sum_{\lambda=1}^{6N} \omega_\lambda^2 = \text{tr}(A^2) = \text{tr}(2\Phi' - W'^2) = -\text{tr}(W'^2), \quad (\text{C6})$$

where we use the fact that  $\Phi'$  is traceless. The stability of the system can as usual be determined by checking if all eigenvalues are real. Noting that the frequencies come in pairs of positive and negative values in the stable regime we can express the above sum in terms of the  $3N$  positive frequencies,

$$\sum_{\lambda=1}^{3N} \omega_\lambda^2 = -\frac{1}{2} \text{tr}(W'^2). \quad (\text{C7})$$

This trace can be explicitly calculated as

$$\begin{aligned} \text{tr}(W'^2) &= -2e^2 B_0^2 \sum_{j=1}^N \frac{1}{m_j^2} \\ &= -2 \sum_{j=1}^N \omega_{c,j}^2, \end{aligned} \quad (\text{C8})$$

where  $\omega_{c,j} = eB_0/m_j$  is the true cyclotron frequency of the  $j$ th ion, thus allowing us to express the sum as

$$\sum_{\lambda=1}^{3N} \omega_\lambda^2 = \sum_{j=1}^N \omega_{c,j}^2. \quad (\text{C9})$$

Note that the sum is independent of the trapping potential. For a typical experiment with ions of the same species and no impurity defects,  $m_j = m$ , and the above sum further simplifies in terms of the common true cyclotron frequency  $\omega_c = eB_0/m$  to

$$\sum_{\lambda=1}^{3N} \omega_\lambda^2 = N\omega_c^2. \quad (\text{C10})$$

Equation C10 can be treated as a non-trivial generalization of the well known Brown-Gabrielse invariance theorem for a single ion in an imperfect Penning trap,

$$\omega_+^2 + \omega_-^2 + \omega_z^2 = \omega_c^2. \quad (\text{C11})$$

One additional result can be derived from equation C2 by using the property that the product of the eigenvalues of a matrix is equal to its determinant so that

$$\begin{aligned} \prod_{\lambda=1}^{6N} \omega_\lambda &= |A| \\ &= \begin{vmatrix} \mathbb{O}_{3N} & \mathbb{I}_{3N} \\ \Phi' & iW' \end{vmatrix}. \end{aligned} \quad (\text{C12})$$

An interchange of  $3N$  columns in the matrix on the r.h.s. allows us to write the product in terms of the  $3N$  positive frequencies as

$$(-1)^{3N} \prod_{\lambda=1}^{3N} \omega_\lambda^2 = (-1)^{3N} \begin{vmatrix} \mathbb{I}_{3N} & \mathbb{O}_{3N} \\ iW' & \Phi' \end{vmatrix}, \quad (\text{C13})$$

or

$$\prod_{\lambda=1}^{3N} \omega_\lambda^2 = |\Phi'|. \quad (\text{C14})$$

Finally, we arrive at

$$\prod_{\lambda=1}^{3N} \omega_\lambda = \sqrt{|\Phi'|}, \quad (\text{C15})$$

which for the case of ions having identical masses can be more conveniently expressed as

$$\prod_{\lambda=1}^{3N} (m\omega_\lambda^2) = |\Phi|. \quad (\text{C16})$$

This result tells us that the product of eigenvalues is independent of the magnetic field and depends only on the curvature tensor of the total electric potential.

### Appendix D: Spin spin coupling

The derivation in this Appendix follows closely the methodology from ref. [29]. The ODF leads to the interaction term

$$\hat{H}_{\text{ODF}} = - \sum_{j=1}^N E_O \cos(\mathbf{k}_R \cdot \mathbf{R}_j - \mu_R t) \hat{\sigma}_j^z. \quad (\text{D1})$$

In the Lamb-Dicke regime, we can expand this expression in terms of the equilibrium positions and deviations from them as

$$\hat{H}_{\text{ODF}} \approx \sum_{j=1}^N E_O \mathbf{k}_R \cdot \hat{\mathbf{r}}_j \sin(\mathbf{k}_R \cdot \mathbf{R}_{j0} - \mu_R t) \hat{\sigma}_j^z. \quad (\text{D2})$$

Then the effective spin Hamiltonian is given by

$$\hat{H}_{\text{SPIN}} = \frac{i}{2\hbar} [\hat{W}_I(t), \hat{V}_I(t)], \quad (\text{D3})$$

which uses the definitions

$$\hat{V}_I(t) = e^{i\hat{H}_{\text{PH}}t/\hbar} \hat{H}_{\text{ODF}}(t) e^{-i\hat{H}_{\text{PH}}t/\hbar}, \quad (\text{D4})$$

$$\hat{W}_I(t) = \int_0^t \hat{V}_I(t') dt' \quad (\text{D5})$$

and

$$\hat{H}_{\text{PH}} = \sum_{\lambda=1}^{3N} \hbar \omega_\lambda (\hat{a}_\lambda^\dagger \hat{a}_\lambda + \frac{1}{2}). \quad (\text{D6})$$

We can express the excursions from equilibrium in terms of the harmonic oscillator creation and annihilation operators, giving

$$\mathbf{k}_R \cdot \hat{\mathbf{r}}_j = -i\hbar \sum_{\nu} k_R^\nu \sum_{\lambda=1}^{3N} (\alpha_{\lambda j \nu}^* \hat{a}_\lambda^\dagger - \alpha_{\lambda j \nu} \hat{a}_\lambda). \quad (\text{D7})$$

In the interaction picture with respect to the oscillator mode Hamiltonian  $\hat{H}_{\text{PH}}$ , we then find that

$$\hat{V}_I(t) = -\frac{\hbar E_O}{2} \sum_{j,\nu,\lambda} k_R^\nu (f_{\lambda j}(t) \alpha_{\lambda j \nu}^* \hat{a}_\lambda^\dagger \hat{\sigma}_j^z - g_{\lambda j}(t) \alpha_{\lambda j \nu} \hat{a}_\lambda \hat{\sigma}_j^z), \quad (\text{D8})$$

where we have defined the functions

$$f_{\lambda j}(t) \equiv e^{i\phi_j} e^{i(\omega_\lambda - \mu_R)t} - e^{-i\phi_j} e^{i(\omega_\lambda + \mu_R)t}, \quad (\text{D9a})$$

$$g_{\lambda j}(t) \equiv e^{i\phi_j} e^{-i(\omega_\lambda + \mu_R)t} - e^{-i\phi_j} e^{-i(\omega_\lambda - \mu_R)t}, \quad (\text{D9b})$$

$$\phi_j = \mathbf{k}_R \cdot \mathbf{R}_{j0}. \quad (\text{D9c})$$

From equations D3, D4 and D5, and making the rotating wave approximation with respect to the oscillator frequencies, we then find that the static part of the effective spin Hamiltonian can be written in the form of an Ising-like spin Hamiltonian

$$\hat{H}_{\text{SPIN}} = \sum_{jj'} J_{jj'}^0 \hat{\sigma}_j^z \hat{\sigma}_{j'}^z, \quad (\text{D10})$$

with the coupling terms given by

$$\begin{aligned} J_{jj'}^0 &= \frac{E_O^2}{2} \sum_{\nu,\nu'} \sum_{\lambda} \frac{\omega_\lambda^2}{m\omega_\lambda^2 + \gamma_\lambda^H \Phi \gamma_\lambda} \frac{k_R^\nu k_R^{\nu'}}{\mu_R^2 - \omega_\lambda^2} \cos(\phi_j - \phi_{j'}) \text{Re}(\gamma_{\lambda j \nu}^* \gamma_{\lambda j' \nu'}) \\ &\quad - \frac{E_O^2}{2} \sum_{\nu,\nu'} \sum_{\lambda} \frac{\omega_\lambda \mu_R}{m\omega_\lambda^2 + \gamma_\lambda^H \Phi \gamma_\lambda} \frac{k_R^\nu k_R^{\nu'}}{\mu_R^2 - \omega_\lambda^2} \sin(\phi_j - \phi_{j'}) \text{Im}(\gamma_{\lambda j \nu}^* \gamma_{\lambda j' \nu'}). \end{aligned} \quad (\text{D11})$$

Here  $\gamma_\lambda$  is the normalized normal mode eigenvector cor-

responding to the frequency  $\omega_\lambda$  and the indices  $\nu, \nu'$  run over  $x, y, z$ .